buildings

MDPI

Article

Relative Evaluation Approach for Cross-Room Exposure in a Detached House Using a Measurement-Informed Multizone Model

Akihiro Katsuki [1,*], Koki Kikuta [2], Yu Tanaka [1], Masato Iguchi [3] and Motoya Hayashi [2]

[1] Graduate School of Engineering, Hokkaido University, Sapporo 0608628, Japan
[2] Faculty of Engineering, Hokkaido University, Sapporo 0608628, Japan; k-kikuta@eng.hokudai.ac.jp (K.K.); motoya.hayashi@eng.hokudai.ac.jp (M.H.)
[3] Department of Architecture, College of Science and Technology, Nihon University, Chiyoda 1018308, Japan; iguchi.masato@nihon-u.ac.jp
* Correspondence: katsuki.akihiro.l4@elms.hokudai.ac.jp

Abstract

Household airborne transmission can be promoted when infectious and susceptible occupants share indoor air for long periods, yet practical infection-risk models often require pathogen-specific parameters that are uncertain. This study proposes a measurement-informed multizone/HVAC-network workflow that identifies inter-room airflow rates (q) from CO_2 tracer time series and estimates an effective first-order non-ventilation aerosol loss rate (λ) by fitting $PM_{2.5}$ concentration decay dynamics; the identified parameters are then reused within the same whole-house recirculating network model (vtsim) to compute a steady-state exhaled-air tracer concentration index for scenario comparison. The workflow is demonstrated in a high-insulation, airtight detached house equipped with a duct-type whole-house air-conditioning system with return-air recirculation. The results indicate measurable cross-room dispersion under baseline operation and show that a return-side filtration scenario reduces the steady-state index in non-source rooms relative to baseline under the tested operating assumptions. These findings illustrate how measurement-informed identification can support rapid, threshold-free relative comparison of ventilation/HVAC operation or mitigation scenarios within a specific house, rather than estimating absolute infection probability. Limitations include potential non-uniqueness in inverse identification, simplified treatment of leakage and pressure-drop-induced airflow changes, and the use of a steady-state index for inherently transient residential exposures; further validation across additional houses and HVAC topologies is warranted.

Keywords: whole-house air-conditioning; cross-room exposure; multizone airflow-network model; exhaled-air tracer concentration; aerosol loss rate

Check for updates

Academic Editor: Constantinos A. Balaras

Received: 5 January 2026
Revised: 23 January 2026
Accepted: 29 January 2026
Published: 30 January 2026

Copyright: © 2026 by the authors. Licensee MDPI, Basel, Switzerland. This article is an open access article distributed under the terms and conditions of the Creative Commons Attribution (CC BY) license.

1. Introduction

Since the COVID-19 pandemic began, the rise in isolation at home has made household transmission a significant public health concern. Many countries legally required isolation at home during the COVID-19 pandemic and imposed fines or criminal penalties for noncompliance [1–3]. Japan did not introduce a general, legally enforceable penalty for isolation at home. Instead, the national and local governments established guidance and support systems for home-based care, and large numbers of patients were managed at home during major waves [4,5]. Household transmission becomes more likely when

infectious and susceptible people share the same indoor space for long periods. Many epidemiological studies in Japan and abroad have documented this [6–9]. Under these circumstances, it is necessary to assess the risk of airborne transmission in homes and to examine infection-control measures through ventilation and HVAC design.

In houses, routine activities such as breathing, talking, coughing, and singing can cause infectious individuals to emit virus-containing aerosols—predominantly fine particles ≤ 5 μm—over time [10]; because these fine aerosols can remain airborne for extended periods, these particles can remain suspended and are transported by indoor airflow, and may migrate beyond the source room to other rooms through inter-room connections and HVAC-driven circulation [11]. Reports detecting SARS-CoV-2 RNA-containing aerosols in rooms of patients under home-based care support the reality of spatial spread in houses [12]. Outdoor-air ventilation rate, inter-room airflow paths, and recirculation practices influence aerosol residence time and the risk of long-range airborne transmission. Adequate ventilation and filtration can help reduce risk beyond close-contact distances (e.g., >1.8 m) [13–15]. Understanding and quantifying aerosol behavior—generation, transport, dilution, deposition, and removal—is essential for estimating exposure potential in homes and for planning and implementing practicable infection-control measures.

Under the ZEH (Net Zero Energy House) initiative, the insulation and airtightness performance of houses has been improved in Japan as part of climate-change mitigation efforts [16]. As sensible loads (thermal loads associated with air-temperature change, excluding latent heat) decrease and humidity-control needs increase, interest and demand have grown for a whole-house air-conditioning system that heats and cools the entire house with a single air-conditioning unit and a large recirculation airflow, rather than room-by-room units [17,18]. Field measurements and analyses show advantages of such systems in reducing temperature nonuniformity, dehumidification performance, and coefficient of performance (COP) [17–19]. Conversely, large recirculation flows and inter-room mixing can provide pathways for transporting infectious aerosols; therefore, design and operational parameters—including outdoor-air ventilation rate, filtration performance, recirculation ratio and airflow paths, and zoning (partitioning the duct/network operation to limit inter-room transport)—must be evaluated and managed systematically [20].

A multizone ventilation network model provides a practical framework to represent inter-room airflows and contaminant transport in residential buildings [21–23]. Aerosols are particulate matter; however, fine aerosols can often be treated as passive scalars for transport, while particle-specific removal processes (deposition and filtration) must be explicitly accounted for. Their concentrations decrease systematically in a size-dependent manner due to deposition (walls, floors, ceilings), gravitational settling, filtration, and other airborne removal processes [24–26]. Some prior studies approximate aerosol losses by adding a bulk removal rate (λ) or filter efficiency to the network model [27]. Other studies introduce size-resolved deposition velocities to describe losses as functions of surface-area ratio and airflow conditions [28]. However, analyses based solely on nominal specifications or forward simulations can deviate from realized behavior because airflow distributions and system operation vary in practice, motivating measurement-informed identification or calibration using concentration time series [29–31]. For aerosols, this challenge is compounded because effective removal can deviate from assumed values under real residential conditions [32,33]. Although inverse estimation of airflow using tracer data and characterization of particle decay/deposition have been reported separately [29–33], house-scale workflows that simultaneously identify both (i) inter-room transport parameters (airflow rates) and (ii) an effective first-order aerosol loss term from measured time series data, and then reuse the identified parameters consistently for scenario evaluation within the same multizone/HVAC-network representation, remain limited in the house scale literature

to our knowledge (Table 1). To address this gap, we employed the ventilation network program vtsim [34], which enables flexible parameterization and inverse identification by fitting multizone/HVAC-network simulations to measured concentration dynamics. In contrast to forward-oriented multizone analyses where loss parameters are typically prescribed, vtsim enables the inverse identification of key parameters by fitting simulated concentration dynamics to measurements. Specifically, we identified unknown inter-room airflow rates using CO_2 tracer measurements and determined an effective first-order aerosol loss rate (λ) from measured particle concentration decay, and then reused the identified model for subsequent case comparisons under the same network representation.

Table 1. Point-by-point comparison of common approaches and the measurement-informed multizone workflow proposed in this study.

Approach Category	Primary Data Used	Identify Inter-Room Airflow (q) from Measurements	Identify Effective Aerosol Loss (λ) from Measurements	Explicit Representation of Recirculating Airflow and Interzonal Flows	Reuse Identified Parameters for Scenario Comparison	Representative References
Forward multizone simulation (prescribed parameters)	Nominal/design inputs	-	-	±	✓	[21–23]
CO_2-based exposure proxy (rebreathed CO_2/CO_2 proxy)	CO_2 only	- (proxy only)	-	-	±	[35]
Inverse multizone using tracer time series (airflow identification)	CO_2/tracer time series	✓	-	±	±	[29–31]
Particle decay/deposition studies (residential PM dynamics)	PM time series	-	✓ (effective decay)	-	-	[32,33]
Multizone with prescribed λ or filter efficiency	Mixed (model + assumed removal)	±	- (assumed)	±	✓	[27,28]
This study (vtsim-based, measurement-informed workflow)	CO_2 + PM time series + operating modes	✓	✓ (effective λ)	✓	✓	This study, [34]

Notes: [✓] indicates explicitly implemented in the referenced approach; [-] indicates not implemented or out of scope; [±] indicates potentially feasible depending on the specific study/implementation (not generally required).

Infection-risk models such as Wells–Riley are useful, but practical applications often require pathogen- and case-specific parameters (e.g., quanta emission rate, viability, and infectious dose), which can be highly uncertain, especially during the early stages of an emerging infectious disease [36–39]. Accordingly, this study does not aim to quantify absolute infection probability or to claim that any single countermeasure is universally optimal. Instead, we present a measurement-informed, exposure-oriented approach for rapid, relative comparison of residential ventilation/HVAC design and operation options without relying on pathogen-specific inputs. This approach identifies inter-room airflow rates from CO_2 tracer measurements and an effective non-ventilation aerosol loss rate from

measured aerosol concentration dynamics; it then computes a steady-state exhaled-air tracer concentration index as a physical surrogate for cross-room exposure potential. By incorporating an effective first-order loss rate (λ), the index accounts for removal processes (e.g., deposition and filtration) in addition to transport and dilution. As summarized in Table 1, the novelty of this work lies in an end-to-end workflow that identifies inter-room airflow rates from CO_2 tracer time series and identifies an effective aerosol loss rate from measured particle concentration dynamics and then reuses the identified parameters within the same whole-house recirculating network model for scenario comparison (case demonstration). A return-side filtration case is included only to demonstrate the approach's comparative capability, rather than to advocate a specific countermeasure or to quantify absolute infection risk.

2. Methods

2.1. Overview of the House

The case house is a detached house in Hokkaido, Japan, equipped with a whole-house air-conditioning system. It has a total floor area of 119.25 m^2, an airtightness C-value of 0.3 cm^2/m^2, and a UA value of 0.17 $W/(m^2 \cdot K)$, indicating a highly insulated and airtight house. Here, the C-value denotes the equivalent leakage area per floor area (cm^2/m^2), and the UA value denotes the overall heat loss coefficient per floor area ($W/m^2 \cdot K$), both commonly used indices in Japan. Figure 1 shows an overview of the whole-house air-conditioning system, and Figure 2 presents the floor plan and the locations of the supply and exhaust outlet (abbreviations: AC = air conditioner; LEV = local exhaust ventilation; 1F/2F = first/second floor; WC = toilet (water closet); UB = bathroom (unit bath); UT = utility room; ACR = air-conditioning room; WIC = walk-in closet).

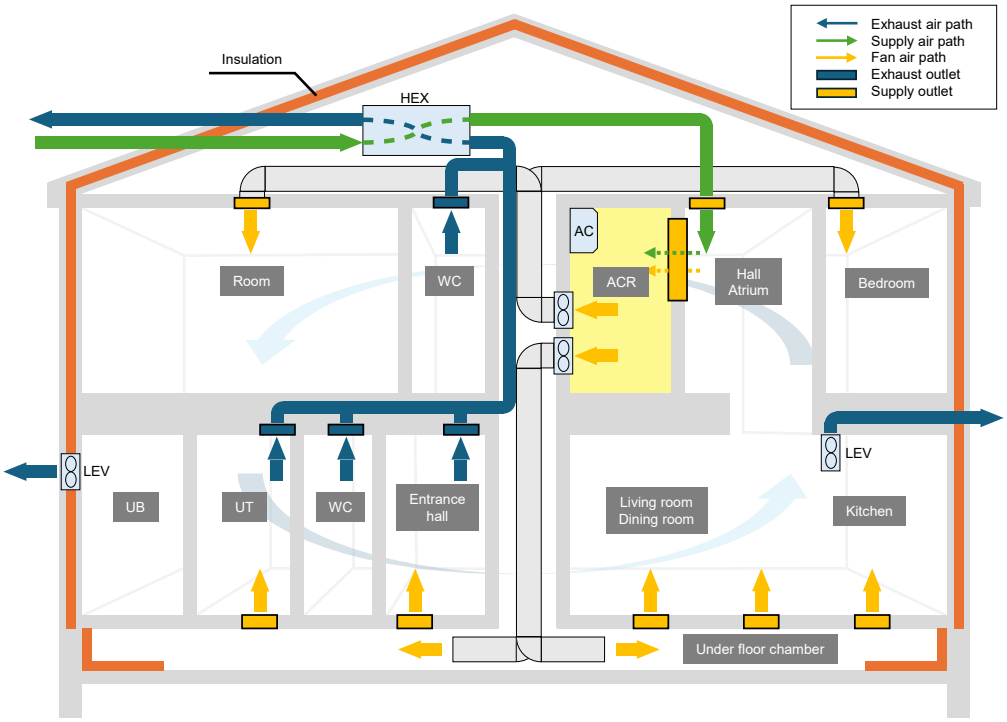


Figure 1. Overview of the whole-house air-conditioning system.

The house employs a balanced ventilation system and performs heat exchange with a total heat exchanger (HEX). Supply air is introduced from the atrium, and exhaust air is extracted from the 1F WC, 2F WC, entrance hall, and corridor. Return air from the rooms mixes in the air-conditioning room (ACR) with outdoor air after heat exchange, and the

air conditioner heats or cools the mixed air. A DC fan delivers the conditioned air to each room through ducts and chambers; air is supplied via the fan outlets (floor grilles on the first floor and ceiling grilles on the second floor) (Figure 2).

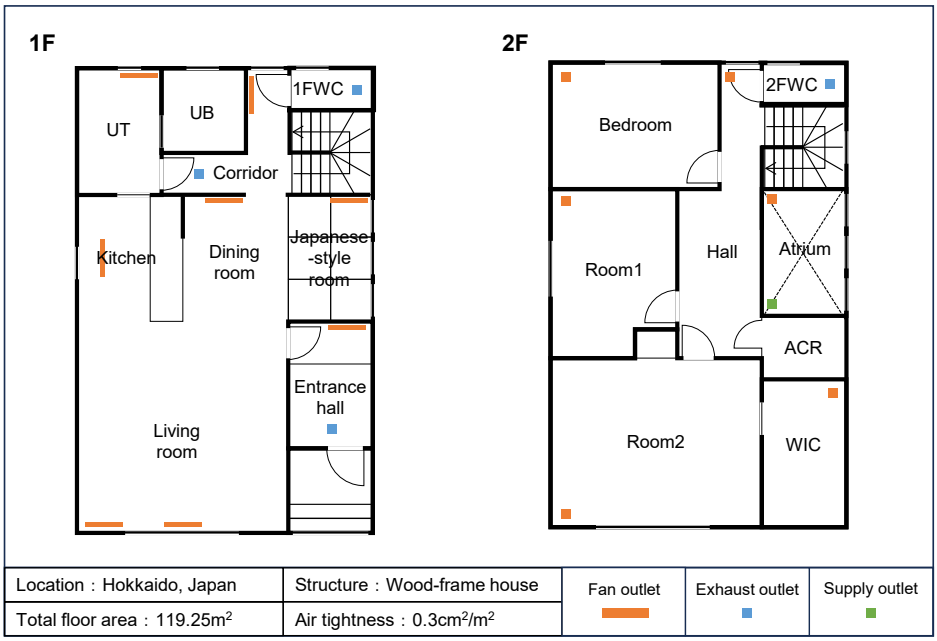


Figure 2. Overview of the house.

Table 2 summarizes the operating conditions and boundary assumptions used for the measurements and identification.

Table 2. Operating conditions and boundary assumptions.

Category	Item	Setting/Value	Notes
Ventilation (outdoor air)	HEX	AVH-95	Operated at level 5 (continuous)
	SA	173 m^3/h	SA was supplied to the atrium
	EA	173 m^3/h	EA was exhausted from 1F WC, 2F WC, corridor, and entrance hall
Whole-house recirculation	Air-distribution fans DC fan	FY-27JDS	DC fans were installed in the ACR
	Fan setting	Low (continuous)	Three speed modes (High/Medium/Low)
	Total recirculating airflow	1861 m^3/h (measured, low setting)	Reported total circulation airflow at weak setting
	Rated airflow (catalog)	FY-27JD8/83 (Panasonic (Osaka, Japan)): L/M/H = 100/200/305 m^3/h	Catalog/reference values
Opening	Interior door	All closed	Pass/undercut exists
	Windows	All closed	-
Airtightness/leakage	Infiltration/exfiltration	Neglected (set to 0)	Explicit modeling assumption for the network model.
	Airtightness reference (C-value)	C = 0.3 cm^2/m^2 (after completion)	reference values

2.2. Modeling Methodology

2.2.1. Modeling Procedure

We built an indoor concentration simulation model using the thermal and ventilation network program vtsim [34]. vtsim is based on a thermal and ventilation network calculation. It operates with nodes, connections, and user-defined conditions. We performed a Newton–Raphson method to minimize the residuals between measured and simulated indoor concentrations and thereby identified the inter-room airflow rates q and the effective non-ventilation aerosol loss rate λ. Here, the aerosol loss rate λ denotes the effective first-order removal rate excluding ventilation, aggregating all non-ventilation loss processes (e.g., deposition/attachment to surfaces and other unmeasured or apparent losses). The Newton–Raphson method was employed because the coupled airflowtransport system is nonlinear, and a Jacobian-based update provides stable and efficient convergence.

Table 3 outlines the model-building procedure. Step 1 constructs Model 1 from the inputs—nodes (room volumes), connections (inter-room paths), and known supply airflow rates. Step 2 involves the identification of the unknown inter-room airflow rates (q) by fitting measured CO_2 concentration dynamics to Model 1 and updating the network to construct Model 2. Step 3 involves the identification of the room-specific aerosol loss rate (λ) by fitting measured aerosol concentration dynamics to Model 2, yielding Model 3, which includes particle losses.

Table 3. Modeling procedure.

	Description	Identified Parameter	Output Model
Step 1	Input of network data (Node: volume, Connection: path and airflow).	-	Model 1
Step 2	Unknown inter-room airflow rates were identified by calibrating the model to measured CO_2 concentration dynamics.	Inter-room airflow rate q	Model 2
Step 3	The aerosol loss rate was identified by calibrating the model to measured aerosol concentration dynamics.	Aerosol loss rate λ	Model 3

2.2.2. Convergence Calculation Procedure

The convergence calculation procedure is shown in Figure 3.

Figure 3 shows the procedure for model construction and parameter identification. In this process, network data (node volumes, airflow connections) were first entered, and a data frame df_i was constructed. The measured concentration data were then loaded as a data frame (df_measurement). In Figure 3, the df_i shown under "Calculate residuals" denotes the simulation outputs recomputed and updated by vtsim at each iteration. The model to be identified at each stage was calibrated against the measured CO_2 or aerosol concentration dynamics. Unknown inter-room airflow rates (q) and the aerosol loss rate (λ) were identified through iterative optimization. During each iteration, the residual vector (ε)—defined as the difference between simulated and measured concentrations—was evaluated, and parameter updates were performed using a Jacobian approximation and LU decomposition to solve the normal equations.

Parameters were updated as follows (example for q):

$$q_{\text{new}} = q_{\text{old}} + \alpha\, \Delta q \tag{1}$$

where α is the relaxation (damping) coefficient controlling the step size of the update. The aerosol loss rate λ was updated in the same manner ($\lambda_{new} = \lambda_{old} + \alpha\Delta\lambda$). Convergence was judged using the root-mean-square error (RMSE) between simulated and measured

concentrations; the iteration was terminated when the change in RMSE between successive steps became smaller than a prescribed threshold (τ). RMSE was used as the objective function and a goodness-of-fit indicator for calibration.

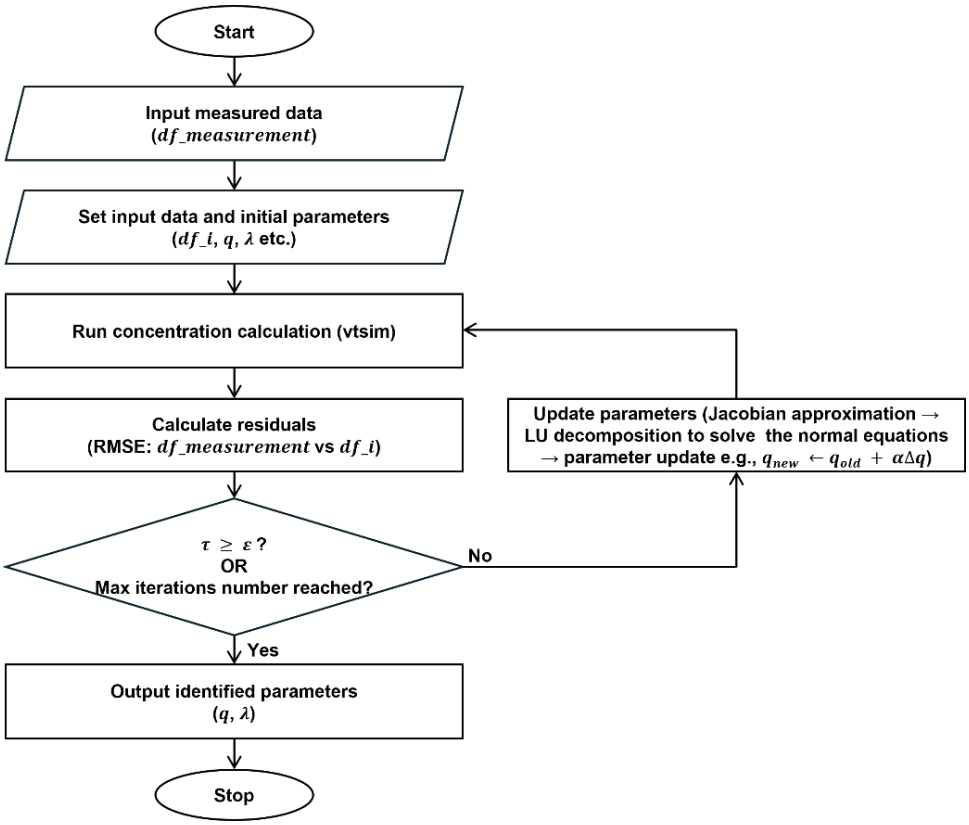


Figure 3. Flowchart of the convergence calculation.

The RMSE is defined as follows:

$$\mathrm{RMSE} = \sqrt{\frac{1}{N}\sum_{k=1}^{N}(\hat{y}_k - y_k)^2} \tag{2}$$

where y_i and $\hat{y}_i$ denote the measured and simulated values, respectively, and N is the number of samples.

The rate of change of particle concentration in room i is given as follows:

$$\frac{dC_i}{dt} = \frac{M_i}{V_i} - \lambda_i C_i + \frac{1}{V_i}\left(\sum_j (1-\eta_{ij}) C_j Q_{ij}^{+} - \sum_j C_i Q_{ij}^{-}\right) \tag{3}$$

where C_i is the tracer concentration in room i [ppm for CO_2; μg/m^3 for aerosols]. The governing equation is identical in form, but for CO_2, the loss terms (β_i, η_{ij}) are set to zero. M_i is the particle release rate in room i [m^3/s or μg/s]; V_i is the room volume [m^3]; λ_i is the aerosol loss rate in room i [1/s]; Q_{ij}^{+} is the airflow rate into room i from room j [m^3/s]; Q_{ij}^{-} is the airflow rate out of room i to room j [m^3/s]; η_{ij} is the dust collection (filtration) efficiency on the path between room i and j; and t is time [s].

The aerosol loss rate λ is determined by the combined action of gravitational settling, Brownian diffusion, and airflow-driven wall impaction, among other processes [40]. In this study, we identified an effective aerosol loss rate λ by fitting the measured aerosol concentration dynamics to the model, thereby aggregating all non-ventilation loss mech-

anisms. However, during the convergence procedure, λ tended to be overestimated in the air-conditioning room (ACR), through which all recirculation flows pass, while λ converged to zero in the other rooms. We therefore constrained λ by imposing a physically motivated lower bound λ_{min}, given by the equation below, and reran the solver to convergence under this constraint. Because we focused on inter-room airborne transport and analyzed $PM_{2.5}$ (particles with relatively long residence times), we derived λ_{min} from the minimum first-order deposition loss expected within the sensor's $PM_{2.5}$ size range (0.3–2.5 μm), considering only gravitational settling and Brownian diffusion. Specifically, λ_{min} was set to the minimum value of the theoretical deposition loss rate over this diameter range, as follows:

$$\lambda_{min} = \frac{U}{H} + \frac{D'S}{\delta V} \tag{4}$$

$$U = \frac{C_m d^2 (\rho_p - \rho) g}{18\mu} \tag{5}$$

$$D' = \frac{C_m k_B T}{3\pi\mu d} \tag{6}$$

where λ_{min} is the theoretical lower bound of the aerosol loss rate [1/s]; U is the terminal settling velocity [m/s]; H is the room height [m]; D' is the diffusion coefficient [m^2/s]; S is the room surface area [m^2]; δ is the boundary-layer thickness [m]; V is the room volume [m^3]; d is the particle diameter [m]; ρ_p is the particle density [kg/m^3]; ρ is the air density [kg/m^3]; g is the gravitational acceleration [m/s^2]; μ is the dynamic viscosity of air [Pa·s]; k_B is the Boltzmann constant [J/K]; and T is the absolute temperature [K]. The terminal settling velocity U is obtained from Equation (5), and the diffusion coefficient D' is determined using Equation (6).

$$C_m = 1 + K_n\left(A + B\exp^{-\frac{C}{K_n}}\right) \tag{7}$$

$$K_n = \frac{2\updownarrow}{d} \tag{8}$$

where C_m is the Cunningham slip correction factor; K_n is the Knudsen number; and $\updownarrow$ is the mean free path of air molecules [m]. The Cunningham correction C_m is obtained from Equation (7), and the Knudsen number K_n is determined using Equation (8). The boundary-layer thickness δ was set to 1.6×10^{-4} [41]. We used the following parameters: A = 1.165, B = 0.483, C = 0.997, and $\updownarrow = 67.3 \times 10^{-9}$ [42].

2.2.3. Input Parameters

We specified the simulation conditions as vtsim node settings (volume, concentration, etc.), connection settings (path, airflow, etc.), and other settings (dust source, air cleaner, etc.). These settings are listed in Table 4.

Table 4. vtsim input parameters.

Category	Parameter	Symbol/Setting	Unit		Description
Node settings (sn)	Concentration flag	*c_flag* (0: none, 1: calc, 2: fixed)	-		Specifies whether concentration is calculated or fixed
	Concentration	c	m^3/m^3	μg/m^3	Initial or fixed concentration
	Room volume	v	m^3		Volume of each zone
	Source Strength	m	m^3/s	μg/s	Release rate from dust source
	Aerosol loss rate	λ	1/s		Represents particle loss (deposition/removal)

Table 4. *Cont.*

Category	Parameter	Symbol/Setting	Unit		Description
Ventilation network (vn)	Flow path	node1- > node2	-		Direction of airflow
	Airflow rate	vol	m^3/s		Supply/exhaust airflow rate through each path
Others	Dust source	dust source	m^3/s	$\mu g/s$	Node and release rate of dust source
	Air cleaner	air cleaner	-		Target path for removal and effi-ciency (η)

2.3. Airflow Measurement Methods

We measured the supply and exhaust airflow rates using an anemometer (KANOMAX, Osaka, Japan; 6750). Direct anemometer measurement of the fan airflow rate in the air-conditioning room was difficult because the room is highly turbulent and narrow. Therefore, we used the tracer-gas method [43]. Specifically, we released CO_2 as a tracer at a constant mass flow from the duct inlet using a mass flow controller (FCON, Kochi, Japan; C1005, 5 SLM-Air), and we measured CO_2 concentrations at the duct outlet and in the air-conditioning room. Using the concentration difference and the CO_2 release rate, we calculated the fan airflow rate according to the following equation:

$$Q = \frac{k}{\Delta C} = \frac{k}{C_i - C_0} \tag{9}$$

where Q is the fan airflow rate [m^3/h]; k is the CO_2 release rate [m^3/h]; C_i is the CO_2 concentration at the duct outlet [m^3/m^3]; and C_0 is the reference (background) concentration measured in the air-conditioning room [m^3/m^3]. Using the measured supply/exhaust airflow rates and the fan airflow rate, we defined the ventilation–recirculation network and constructed Model 1.

2.4. Measurements of CO_2 and Aerosol Dynamics

We measured the CO_2 concentration and aerosol concentrations used for identification in Steps 2 and 3. We placed a CO_2 logger (T&D, Nagano, Japan; TR-76Ui) and a PM sensor (Watty, Tokyo, Japan; HYPM) at approximately 1.2 m above the floor near the room center. The PM sensor is based on a laser light-scattering method and reports PM mass concentrations for size fractions $PM_{1.0}$ (0.3–1.0 μm), $PM_{2.5}$ (0.3–2.5 μm), $PM_{4.0}$ (0.3–4.0 μm), and PM_{10} (0.3–10 μm). The measurement range is 0–1000 $\mu g/m^3$, with a stated accuracy of ±10 $\mu g/m^3$ for 0–100 $\mu g/m^3$ and ±10% for 100–1000 $\mu g/m^3$ (±15% at ≤10 °C or ≥40 °C) [44]. Concentrations were logged at 1 min intervals. As measurement conditions, we set the total heat exchanger (HEX) to its minimum setting and stopped the DC fan in the air-conditioning room before starting the measurement. In the bedroom, we released CO_2 gas and aerosols for 3 min and then returned the HEX and the DC fan to normal operation. During the measurement, we kept all room doors closed and recorded data for 1 h. After the measurement, we retrieved the data from all the devices. We generated aerosols using a nebulizer (Omron, Kyoto, Japan; NE-C28) by nebulizing an oral rehydration solution (Otsuka Pharmaceutical, Tokyo, Japan; OS-1). According to the manufacturer's specifications, the nebulizer produces an aerosol with a mass median aerodynamic diameter (MMAD) of approximately 3 μm and a nebulization rate of 0.4 mL/min (aerosol output 0.4 mL) [45]. The generated aerosol was used as a physical tracer for particle transport and loss, rather than as a direct surrogate for infectious virus. OS-1 was selected because it is safe for use in occupied buildings and has been adopted in

Japanese field studies of aerosol dispersion [46]. Prior reports have used non-hazardous surrogate aerosols (e.g., salt particles) to mimic the spreading and removal behavior of virus-laden aerosols in indoor environments; therefore, we used OS-1 as a practical tracer aerosol in transport tests [47].

2.5. Calculation Method for the Exhaled-Air Tracer Concentration

Infection risk is considered to be related to the inhaled viral dose, which depends on both the airborne virus concentration and the duration of exposure. The amount of virus contained in exhaled breath varies greatly with factors such as virus type, symptom severity, and the immune status of the infected individual. Moreover, the quantitative relationship between the inhaled viral dose and the actual infection risk has not yet been clarified. Therefore, instead of relying on the infection quanta emission rate as in probabilistic infection models (e.g., the Wells–Riley equation), this study used the exhaled-air tracer concentration formed when a single infected person's exhalation is treated as a constant source. This concentration was employed as a relative indicator of exposure potential in indoor air environments.

The time variation of the exhaled-air tracer concentration in each room is expressed by Equation (3) based on the multizone ventilation network model. Under steady-state conditions ($dC_i/dt = 0$), the steady concentration in room i, C_i^{steady}, is calculated by the following equation:

$$C_i^{steady} = \frac{M_i + \sum_j (1 - \eta_{ji}) C_j Q_{ji}}{\lambda_i V_i + \sum_j Q_{ij}} \tag{10}$$

Assuming that one infected person is present in the bedroom, we assigned a constant release rate, M_i, and computed the steady-state concentration C_i^{steady} in each room using the ventilation-network program vtsim. We then used the computed steady concentrations as a relative indicator of exposure potential in indoor air environments. Because the method evaluates the exhaled-air tracer concentration itself, it does not rely on pathogen-specific infection thresholds or probabilistic infection models. It therefore enables quantitative, relative evaluation of infection-control measures' effectiveness based on ventilation conditions and the indoor environment. In addition, since it is grounded in room concentrations originating from exhalation, the method retains generality and can be applied in the early phase of emerging or re-emerging epidemics for like-for-like comparison and verification.

3. Results

3.1. Results of Airflow Measurements and the Ventilation–Recirculation Network (Step 1)

Based on the measured supply and exhaust airflow rates, the computed inter-room airflow rates, and the connection/path information, we constructed the ventilation–recirculation network (Figure 4). Among the inter-room airflow rates shown in the figure, several paths ($q(0)$–$q(3)$) could not be obtained directly from measurements and were therefore treated as unknowns to be identified in Step 2.

3.2. Identification of Inter-Room Airflow Rates (Step 2)

In Step 1, the supply and exhaust airflow rates and the fan flow rates were measured, and the overall airflow balance was checked for consistency. However, several inter-room airflow rates could not be measured. Accordingly, in Step 2, we calibrated Model 1 to the measured CO_2 concentration dynamics to identify the unknown inter-room airflow rates and thereby constructed Model 2. Within vtsim, the variables $q(0)$–$q(3)$ (Figure 4) were treated as parameters to be identified; we minimized the RMSE between simulated and measured concentrations to estimate the inter-room airflow rates.

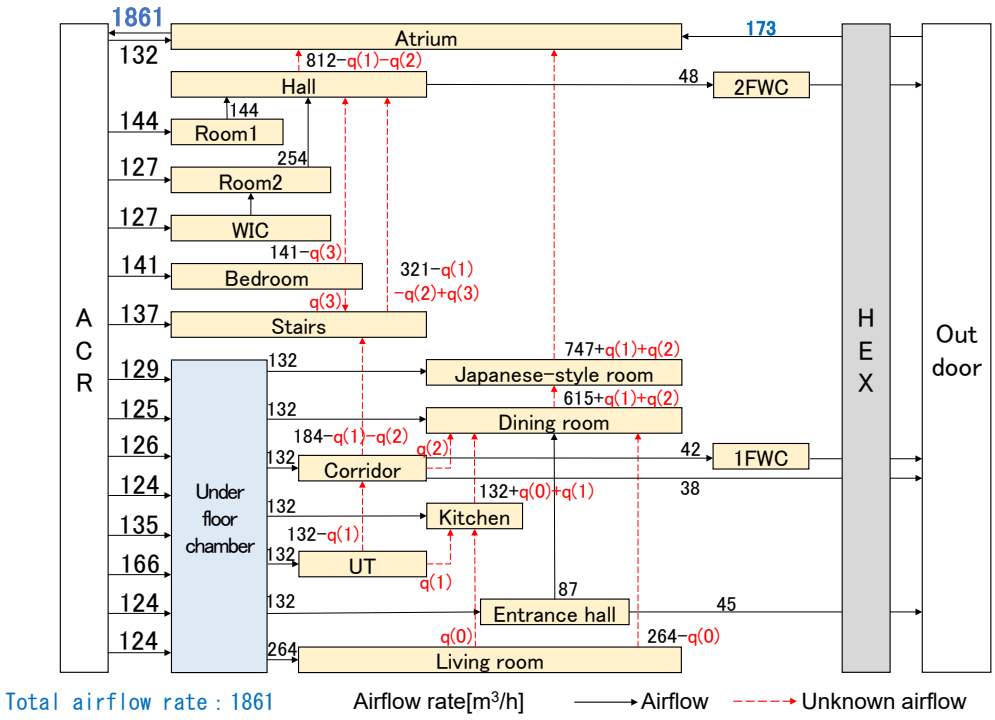


Figure 4. Ventilation–recirculation network (Model 1).

Figure 5 presents the comparison between measured and simulated concentrations at 15 measurement points, and Figure 6 shows the ventilation–recirculation network of Model 2.

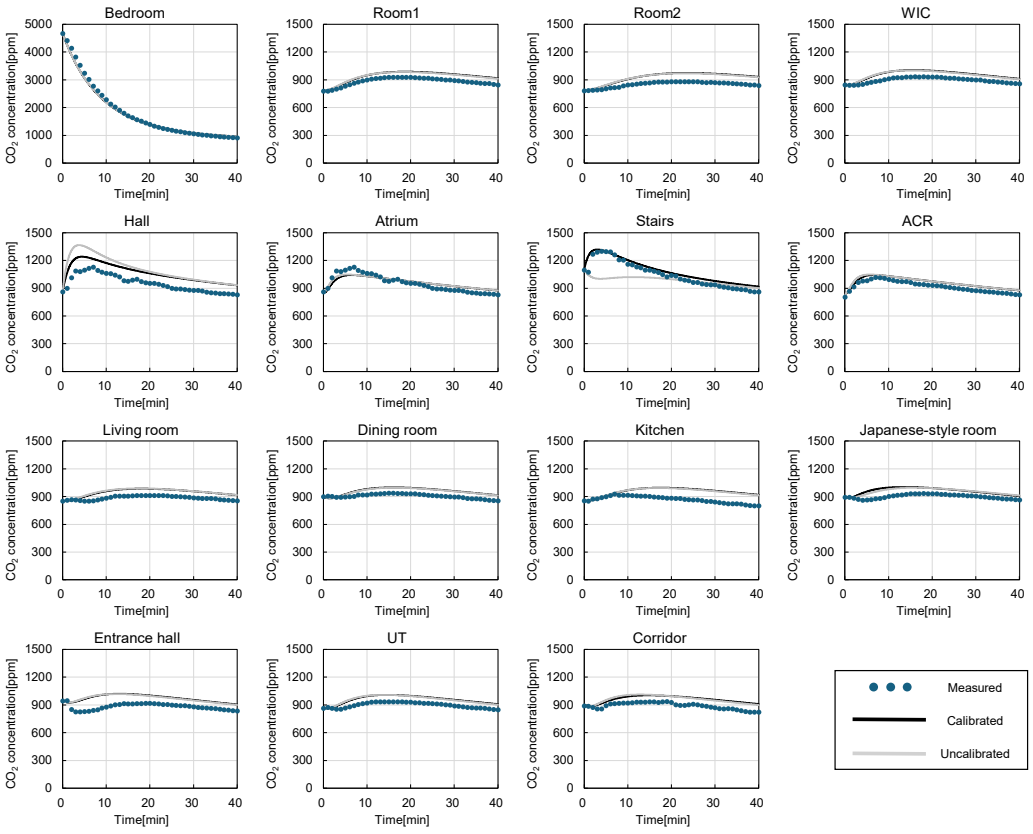


Figure 5. Comparison between measured and simulated concentrations (CO_2).

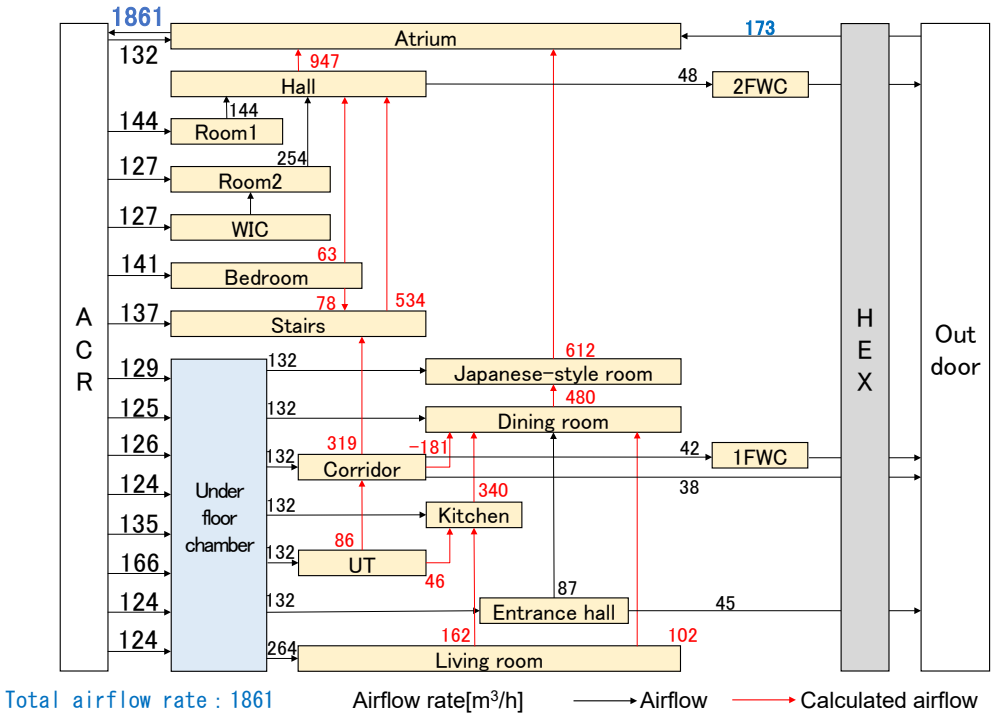


Figure 6. Ventilation–recirculation network (Model 2).

3.3. Identification of the Aerosol Loss Rate (Step 3) and Verification of Model Applicability

Using Model 2 constructed in Step 2, we calibrated the model against the measured aerosol concentration dynamics and identified the aerosol loss rate λ for each room. The identified values are summarized in Table 5. The identified effective non-ventilation aerosol loss rate (λ) was of similar magnitude across rooms under the present experimental conditions. These values serve as effective parameters for reproducing aerosol dynamics under the present conditions.

Table 5. Aerosol loss rates.

Room	Aerosol Loss Rate λ [1/s]
ACR	0.0000018
Living room	0.0000017
Bedroom	0.0000018
Room 1	0.0000018
Room 2	0.0000018
Japanese-style room	0.0000017

Figure 7 compares aerosol concentrations from measurements and simulations. Concentration calculated with Model 3 showed adequate agreement with the measurements, confirming the validity of the identification. To examine model generality, we conducted an additional measurement with the release source relocated from the bedroom to the living room and performed a simulation with Model 3 under the same settings; the results are shown in Figure 8. The simulation again agreed well with the measurements, indicating that the model is applicable under different source locations/conditions. As a quantitative method, the agreement between simulations and measurements was evaluated using RMSE (Equation (2)).

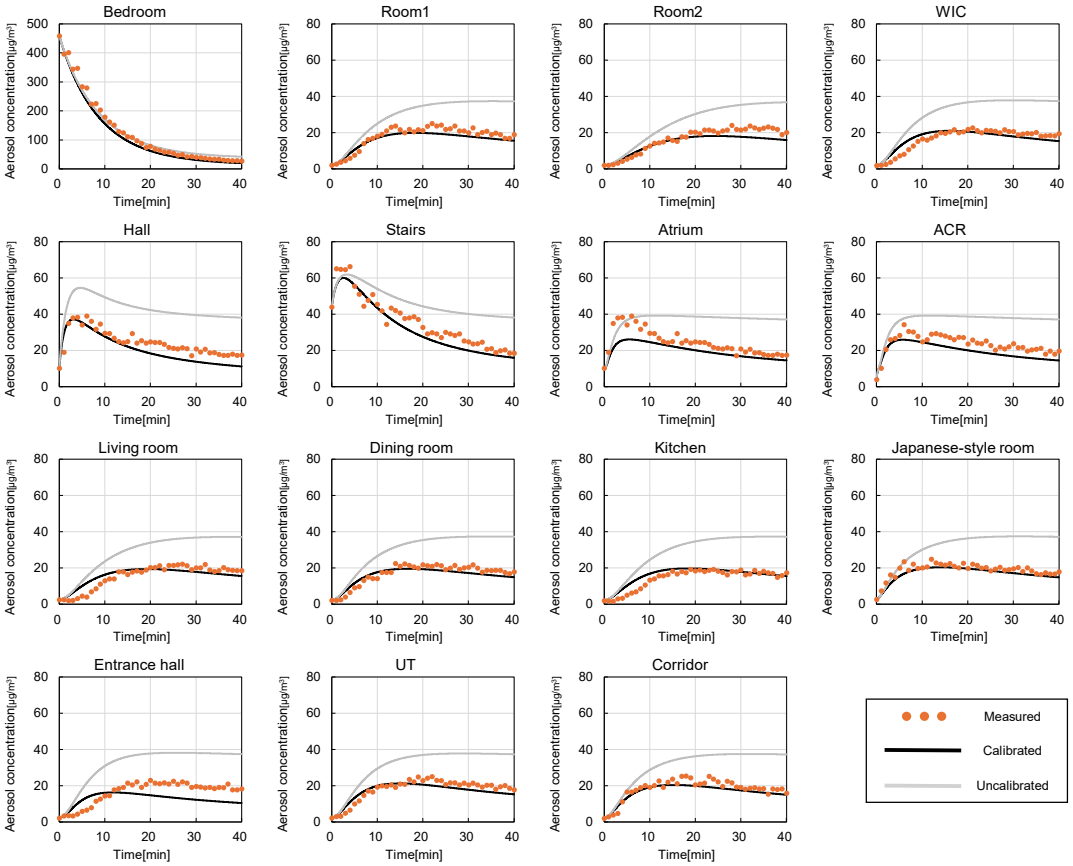


Figure 7. Comparison between measured and simulated concentrations (aerosol).

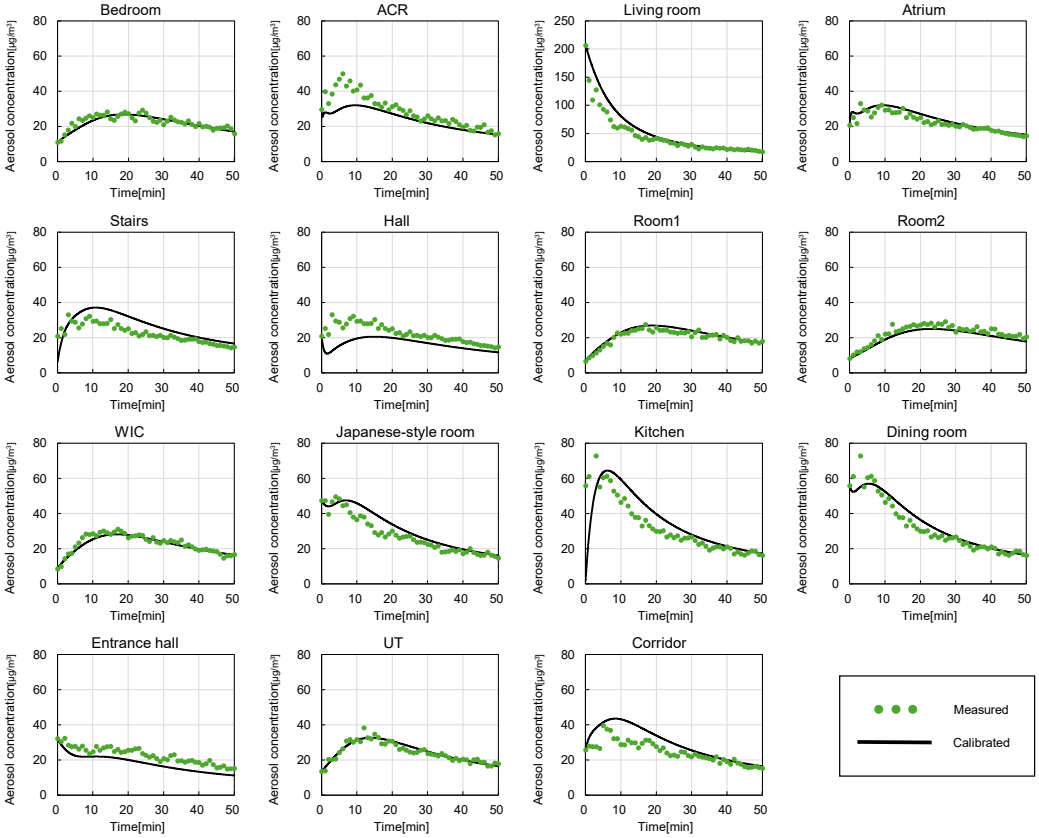


Figure 8. Comparison between measured and simulated concentrations (source: living room).

Table 6 summarizes the RMSE between measurements and simulations for each model. For CO_2, the RMSE decreased from 85 ppm to 75 ppm after calibration (Model 2). Given the CO_2 logger accuracy (±50 ppm or ±5% of reading, whichever is greater), the remaining discrepancy is within—or comparable to—expected measurement uncertainty, suggesting that further reductions may be constrained by measurement noise and unmodeled dynamics. For the bedroom-source aerosol case, the RMSE improved from 14.4 μg/m^3 to 5.6 μg/m^3, demonstrating the validity of Model 3. For the living-room source scenario, the RMSE was 6.4 μg/m^3, showing similarly good agreement under a different source location within the same house and operating modes. Because Model 3 is calibrated directly to the PM mass concentration time series, the achievable agreement is inherently bounded by the instrument-stated PM measurement accuracy (±10 μg/m^3 for 0–100 μg/m^3, and ±10% for 100–1000 μg/m^3; ±15% at ≤10 °C or ≥40 °C). Therefore, the remaining discrepancies should be interpreted as a combination of measurement uncertainty and model simplifications (e.g., room-mean representation, spatial non-uniformity, and unmodeled sinks). Taken together, these results support the consistency of Model 3 for relative, measurement-informed comparisons across the tested source locations, while not implying universal applicability beyond the present case-study setting.

Table 6. RMSE values.

Source Room	Index	Before Calibration	After Calibration
Bedroom	CO_2 [ppm]	85	75
	Aerosol [μg/m^3]	14.4	5.6
Living room	Aerosol [μg/m^3]	-	6.4

3.4. Exhaled-Air Tracer Concentration

By comparing the steady-state exhaled-air tracer concentration, we examined a method to evaluate in-room dispersion behavior and the effectiveness of infection-control measures. The bedroom occupied by the infected individual was treated as the isolation room (source room), and two cases were analyzed, as described below.

Case 1 assumes standard operation of the whole-house air-conditioning system. The supply–exhaust balance and recirculation airflow were maintained under normal operating conditions, and no additional infection-control measures were implemented. Case 2 assumes that the bedroom occupied by the infected person functions as an isolation room. Based on the configuration of Model 3, a high-efficiency filter was introduced into the return-air path from the isolation room (bedroom) to the air-conditioning room. The thermal environment and recirculation airflow provided by the whole-house air-conditioning system were assumed to be maintained, while air inflow from the isolation room to other rooms was suppressed, and the pressure balance was preserved. In this study, the return-path filter was assumed to be a HEPA (high-efficiency particulate air) filter with a collection efficiency of η = 99.95%. HEPA filters exhibit high capture performance even at the most penetrating particle size (MPPS, ≈0.3 μm) and provide sufficient removal capacity under the return airflow of 150 m^3/h considered here.

In all cases, a single infected individual was assumed to stay in the isolation room for an extended period. The exhalation flow rate, representing the emission source, was fixed at 6 L/min, corresponding to normal breathing.

Table 7 lists the steady-state exhaled-air tracer concentrations in each room. In Case 1, exhaled air released in the source room dispersed to other rooms, resulting in elevated concentrations throughout the house. In Case 2, the return-path filter captured a portion of the exhaled-air tracer circulated through the HVAC network, and the average concentration in non-source rooms decreased by approximately 85% relative to Case 1 under the tested

operating conditions. These room-by-room steady-state concentrations are used here as a relative indicator of cross-room exposure potential for comparing ventilation/HVAC countermeasures, rather than for estimating absolute infection probability or relying on infection thresholds.

Table 7. Steady-state exhaled-air tracer concentrations [ppm].

Room	Case 1 [ppm]	Bounds	Case 2 [ppm]	Bounds	Reduction (Relative to Case 1) [%]
ACR	402.1	361.9–442.3 (±10%)	58.6	48.6–68.6 (±10%)	85.4
Living room	401.5	361.4–441.7 (±10%)	58.5	48.5–68.5 (±10%)	85.4
Dining room	385.1	346.6–423.6 (±10%)	56.1	46.1–66.1 (±10%)	85.4
Kitchen	397.1	357.4–436.8 (±10%)	57.9	47.9–67.9 (±10%)	85.4
Room 1	401.4	361.3–441.5 (±10%)	58.5	48.5–68.5 (±10%)	85.4
Room 2	401.4	361.0–441.2 (±10%)	58.4	48.4–68.4 (±10%)	85.5
Bedroom	3020.8	2718.7–3322.9 (±10%)	2683.8	2415.4–2952.2 (±10%)	11.2

To provide a first-order uncertainty characterization consistent with the measurement-informed workflow, we report uncertainty bands for the steady-state concentrations based on the instrument-stated PM measurement accuracy used in Model 3 calibration (reported as conservative bounds rather than statistical confidence intervals). These bands reflect measurement accuracy only and do not capture additional uncertainties such as airflow-rate uncertainty, sensor placement/representativeness, or model-structure uncertainty.

4. Discussion

4.1. Dispersion Risk in Recirculating Duct-Type Whole-House Air-Conditioning Systems

The filtration scenario in this study is presented only as a demonstration of the proposed measurement-informed multizone evaluation approach; the main contribution is the workflow for identifying inter-room transport and enabling rapid, relative comparison of design/operation options without relying on pathogen-specific parameters. Under normal recirculating operation (Case 1), the non-source rooms exhibited a non-negligible steady-state exhaled-air tracer concentration, indicating that the duct network and recirculation can promote inter-room mixing and cross-room transport in this configuration. This finding is consistent with the general understanding that contaminant fate indoors is governed by interzonal airflows, recirculation pathways, and removal processes such as filtration and deposition. In the demonstration case (Case 2), introducing a return-side high-efficiency filter reduced the steady-state tracer concentration in non-source rooms substantially, illustrating how the proposed approach can quantify the relative effect of a mitigation option within a given house and HVAC configuration. Importantly, the magnitude of reduction should be interpreted as case- and implementation-dependent: actual performance may be influenced by non-idealities such as filter bypass, duct leakage, infiltration/exfiltration, and changes in system operating point after filter installation (e.g., airflow reductions due to added pressure drop) [48].

In addition, this case illustrates why a measurement-informed workflow is valuable in practice: flow distributions and realized operating conditions can deviate from nominal specifications, and such deviations can materially affect cross-room transport and the relative performance of operational options. Accordingly, the present discussion focuses on interpreting the measured-house results and on the proposed comparison workflow, rather than on prescribing a universally optimal countermeasure.

4.2. Positioning of the Concentration Index for Relative Evaluation

Airborne infection risk depends on pathogen emission, viability, host susceptibility, activity, and time-varying exposure. In contrast, the exhaled-air tracer concentration index used here is intended as a physical surrogate for cross-room exposure potential, not as a direct measure of infection probability. CO_2 has been widely used as a proxy for rebreathed air to interpret exposure to exhaled air in indoor environments, providing a practical basis for comparing ventilation and air-cleaning strategies when pathogen-specific parameters (e.g., quanta emission rate or infectious dose) are uncertain or unavailable [49]. Accordingly, this study focuses on relative evaluation: under comparable occupancy and source assumptions, relative changes in the steady-state exhaled-air tracer concentration can be interpreted as relative changes in long-term average exposure potential attributable to ventilation/HVAC conditions and mitigation options. Nevertheless, steady-state is an idealization for residential settings where transient emissions, door operations, and HVAC cycling can be important [50–52]; therefore, the present index should be interpreted as a design-oriented or long-term-average comparator rather than a predictor of short-term peaks or near-field exposure.

For aerosols, we identified an effective non-ventilation aerosol loss rate (λ) from measured concentration dynamics, aggregating multiple loss mechanisms (e.g., deposition, size-dependent measurement losses, and other unmeasured sinks) into a first-order term. This "effective" λ is not necessarily equal to a purely physical deposition rate for each room, and the convergence behavior (overestimation in the air-conditioning room and near-zero values elsewhere) indicates practical identifiability limitations when calibrating a simplified loss parameter from room-mean $PM_{2.5}$ measurements. The imposed lower bound (λ_{min}) serves as a physically motivated regularization to exclude nonphysical solutions while maintaining the intended purpose of the approach: robust relative comparison of scenarios within a measured house–HVAC system.

Notably, the identified λ values in Table 5 are very small in magnitude ($\approx$1.7–1.8 $\times$ 10^{-6} s^{-1}, i.e., $\approx$0.006–0.007 h^{-1}), and several rooms effectively converged to the imposed lower bound, λ_{min}, indicating that λ was not strongly identifiable from the available room-mean PM time series under the adopted simplified representation. Because λ is defined here as a non-ventilation effective loss term, it should not be directly compared with "total decay constants" reported in PM decay studies unless ventilation removal is explicitly included (i.e., total decay = ventilation + λ).

Although the present study intentionally avoids pathogen-specific assumptions, the proposed tracer-based index can, in principle, be linked to disease-specific infection risk models when the relevant parameters become available. By combining the predicted inhalation exposure (e.g., time-integrated rebreathed-air fraction) with external information such as pathogen concentration in exhaled air and dose–response (or quanta-based) relationships, one may estimate scenario-dependent infection risk for a given exposure duration. Such estimates, however, would remain highly uncertain and should be interpreted as approximate, because infection outcomes depend on large inter-individual variability (susceptibility, immune status) and other factors not represented in the present framework.

4.3. Interpretation and Robustness of the Effective Loss Rate λ

In this study, λ_{min} was derived as a conservative minimum deposition-related loss within the 0.3–2.5 µm size range (where deposition can be minimized around the lower end of this range), and it was used as a stabilizing bound when the inverse identification tended to drive λ toward near-zero values. Therefore, the small λ values reported for several rooms primarily reflect a regularized lower-bound estimate rather than uniquely determined physical deposition rates. This modeling choice is also linked to the tested HVAC topology: a whole-house recirculating system in which air repeatedly passes through the HVAC/air-

handling room, so the effective removal represented by λ can be strongly influenced by processes along the recirculation path and by the measurement/sampling configuration.

Because the primary goal is relative comparison within the same measured house–HVAC network, the workflow is intended to be most reliable when scenario differences are dominated by changes in transport and/or removal that are well represented in the identified model. A systematic sensitivity analysis of scenario ranking to plausible λ ranges (and to uncertainties in q and source strength) was not conducted here; this remains an important next step to demonstrate robustness of scenario ordering under uncertainty.

4.4. Mitigation Is Not Elimination: Practical Implications and Limitations

Even with a high-efficiency return-side filter, dispersion was not eliminated in the present demonstration. This is expected because filtration is only one component of exposure control, and residual transport can persist via imperfect mixing, short-circuiting, leakage/infiltration pathways, and time-varying operation [53–56]. Moreover, adding high-efficiency filtration can increase pressure drop and alter airflow rates and pressure balance, potentially affecting both thermal performance and contaminant transport; therefore, practical implementation requires consideration of fan capability, operating point changes, bypass leakage control, and maintenance (e.g., loading) [57–60]. These considerations motivate fundamental design principles for residential infection control beyond "adding a filter," including controlling airflow directionality between rooms, ensuring adequate outdoor-air ventilation, providing dedicated exhaust for source spaces when feasible, and adopting measurement-informed commissioning to verify intended performance.

Overall, the proposed approach is best viewed as a diagnostic-and-comparison workflow that can support such commissioning and design decisions by quantifying cross-room exposure potential under defined operating modes, rather than as a tool for asserting absolute infection risk or universally optimal measures.

4.5. Limitations and Applicability

The inverse identification of inter-room airflow rates (q) and an effective aerosol loss rate (λ) is not guaranteed to yield a unique solution. Multiple parameter sets can reproduce the measured concentration time series with similar goodness-of-fit, particularly when measurement noise, unmodeled dynamics, and model simplifications are present. Therefore, the identified parameters should be interpreted as effective values conditional on the adopted model structure and operating assumptions. Their plausibility should be checked by comparing model-measurement residuals with expected measurement errors and, when possible, by validation against independent measurements or alternative operating periods. In some cases, additional constraints or regularization (e.g., bounds derived from physical considerations) are needed to avoid non-physical solutions. In this study, because λ aggregates multiple sinks (deposition, filtration, sampling losses, and other unmodeled removal), we introduced a lower bound (λ_{min}) based on an assumed minimum deposition rate to stabilize the identification and avoid unrealistically small losses. This choice is pragmatic rather than universal: λ_{min} is not a required component of the proposed workflow, and alternative constraints (or no lower bound) may be appropriate depending on the building, instrumentation, operating conditions, and target particle size range. Moreover, the present case is a whole-house recirculating system in which air repeatedly passes through the HVAC/air-handling room; thus, the identified λ is particularly influenced by removal along the recirculation path. Accordingly, the present identification settings and resulting parameter values should be viewed as a case-study implementation for this specific system.

The nebulizer aerosol had a reported MMAD on the order of a few micrometers (≈3 μm), whereas λ was identified using room-mean $PM_{2.5}$ dynamics as a practical measurement surrogate. This particle-size mismatch may bias the effective λ because deposition and filtration are size-dependent, and a single first-order λ cannot fully represent size-resolved fate processes. In addition, the use of an oral rehydration solution (OS-1) for nebulization can affect drying and crystallization behavior, potentially altering the resulting dry particle size distribution relative to human respiratory aerosols. These factors introduce uncertainty in mapping the experimental aerosol to a single effective λ and should be considered when interpreting absolute values, while the present work emphasizes relative comparison within the tested setup.

Uncertainties in airflow rates, tracer release rates, sensor placement, and model structure can affect both the identified parameters and the derived steady-state exhaled-air tracer concentration index. While the present study emphasizes a measurement-informed workflow and relative scenario comparison, a full uncertainty propagation analysis (e.g., Monte Carlo simulation) was not conducted across all uncertain inputs. Consequently, the reported exposure index values should be interpreted as estimates conditional on the adopted assumptions, and the robustness of scenario ranking under plausible uncertainty ranges should be further examined in future work. A practical next step is to propagate uncertainty in q, λ, and source strength through the steady-state index and report uncertainty bands on scenario differences.

Residential exposures are inherently transient due to door opening/closing, occupant movement, intermittent source emissions, and HVAC operational cycling. The steady-state exhaled-air tracer concentration used here is intended as a comparative metric for scenario ranking under the tested operating modes, rather than as a direct representation of time-varying exposure in real households. Therefore, the practical interpretation should be limited to relative comparisons under controlled conditions, and the extent to which scenario ranking persists under typical transient behaviors remains an open question for future studies.

Filtration performance was represented by an effective efficiency term in the modeled recirculation path. In practice, realized filtration effectiveness can depend on bypass leakage, installation quality, and pressure-drop-induced flow changes interacting with the fan curve, particularly in residential systems. If airflow is reduced by filter pressure drop, both transport and removal can change concurrently. Although the filtration case in this study is included to demonstrate comparative capability rather than to advocate a specific countermeasure, future work should explicitly quantify filter-induced flow changes and evaluate a range of effective efficiencies to better represent field performance.

The present results are based on a single detached house with one HVAC topology and a specific airtightness/operational setting. Therefore, general claims should be avoided: the findings primarily demonstrate the proposed measurement-informed workflow and its use for relative scenario comparison in this particular system. To establish transferability, additional cases are needed with varying key determinants such as HVAC topology (e.g., different recirculation architectures), building airtightness and leakage distribution, door configurations, and operating modes across seasons.

5. Conclusions

This study presented a measurement-informed multizone evaluation approach for the relative assessment of inter-room airborne transport and mitigation performance in residential environments. By identifying inter-room airflow rates from CO_2 tracer measurements and an effective non-ventilation aerosol loss rate from measured aerosol concentration dynamics, the approach enables rapid quantification of the relative impacts of

ventilation and air-conditioning design/operation options without relying on pathogen-specific thresholds.

As a demonstration in a detached house equipped with a duct-type whole-house air-conditioning system with recirculation, the identified model indicated measurable inter-room dispersion under normal operation. In contrast, a return-side filtration scenario substantially reduced the steady-state exhaled-air tracer concentration in non-source rooms. These case results are presented to illustrate the approach's comparative capability rather than to advocate a specific countermeasure.

The present model centers on concentration calculations identified from measurements and does not fully account for coupled thermal circuits, pressure differentials, leakage, or transient operations. Future work will incorporate coupled thermal-pressure modeling and additional validations across different house layouts and HVAC configurations to assess dispersion-control strategies more rigorously.

Author Contributions: Conceptualization, A.K., K.K. and M.H.; methodology, A.K., K.K. and M.H.; validation, A.K. and Y.T.; investigation, A.K. and Y.T.; writing—original draft preparation, A.K.; writing—review and editing, all authors; visualization, A.K.; supervision, K.K., M.I. and M.H. All authors have read and agreed to the published version of the manuscript.

Funding: This research received no external funding.

Data Availability Statement: The original contributions presented in this study are included in the article. Further inquiries can be directed to the corresponding author.

Acknowledgments: This research was carried out in collaboration with Hokkaido University and Nihon University. The authors gratefully acknowledge their support and cooperation.

Conflicts of Interest: The authors declare no conflicts of interest.

References

1. Department of Health and Social Care. New Legal Duty to Self-Isolate Comes into Force Today. 2020. Available online: https://www.gov.uk/government/news/new-legal-duty-to-self-isolate-comes-into-force-today (accessed on 28 October 2025).
2. Ministry of Health (Singapore). Promulgation of Regulations Under Infectious Diseases Act [Press Release]. Ministry of Health Singapore. 2020. Available online: https://www.moh.gov.sg/newsroom/promulgation-of-regulations-under-infectious-diseases-act/ (accessed on 28 October 2025).
3. New Zealand Government. COVID-19 Public Health Response (Self-Isolation Requirements) Order 2022 [Revoked August 15, 2023]. New Zealand Legislation. 2022. Available online: https://www.legislation.govt.nz/regulation/public/2022/0046/latest/contents.html (accessed on 28 October 2025).
4. Ministry of Health, Labour and Welfare (Japan). COVID-19 Q&A: Self-Isolation and Close Contact. Available online: https://www.mhlw.go.jp/stf/covid-19/qa.html (accessed on 28 October 2025).
5. Ministry of Health, Labour and Welfare (Japan). Open Data (COVID-19). Available online: https://www.mhlw.go.jp/stf/covid-19/open-data_english.html (accessed on 28 October 2025).
6. Madewell, Z.J.; Yang, Y.; Longini, I.M., Jr.; Halloran, M.E.; Dean, N.E. Household transmission of SARS-CoV-2: A systematic review and meta-analysis. *JAMA Netw. Open* **2020**, *3*, e2031756. [CrossRef]
7. Lewis, N.M.; Chu, V.T.; Ye, D.; Conners, E.E.; Gharpure, R.; Laws, R.L.; Reses, H.E.; Freeman, B.D.; Fajans, M.; Rabold, E.M.; et al. Household Transmission of Severe Acute Respiratory Syndrome Coronavirus-2 in the United States. *Clin. Infect. Dis.* **2020**, *73*, e1805–e1813. [CrossRef]
8. McLean, H.Q.; Grijalva, C.G.; Hanson, K.E.; Zhu, Y.; Deyoe, J.E.; Meece, J.K.; Halasa, N.B.; Chappell, J.D.; Mellis, A.M.; Reed, C.; et al. Household Transmission and Clinical Features of SARS-CoV-2 Infections. *Pediatrics* **2022**, *149*, e2021054178. [CrossRef]
9. Ogata, T.; Irie, F.; Ogawa, E.; Ujiie, S.; Seki, A.; Wada, K.; Tanaka, H. Secondary Attack Rate among Non-Spousal Household Contacts of Coronavirus Disease 2019 in Tsuchiura, Japan, August 2020–February 2021. *Int. J. Environ. Res. Public Health* **2021**, *18*, 8921. [CrossRef]
10. Adenaiye, O.O.; Lai, J.; de Mesquita, P.J.B.; Hong, F.; Youssefi, S.; German, J.; Tai, S.H.S.; Albert, B.; Schanz, M.; Weston, S.; et al. Infectious Severe Acute Respiratory Syndrome Coronavirus 2 (SARS-CoV-2) in Exhaled Aerosols and Efficacy of Masks During Early Mild Infection. *Clin. Infect. Dis.* **2021**, *75*, e241–e248. [CrossRef] [PubMed]

11. Morawska, L.; Cao, J. Airborne transmission of SARS-CoV-2: The world should face the reality. *Environ. Int.* **2020**, *139*, 105730. [CrossRef] [PubMed]
12. Correia, G.; Rodrigues, L.; Afonso, M.; Mota, M.; Oliveira, J.; Soares, R.; Tomás, A.L.; Reichel, A.; Silva, P.M.; Costa, J.J.; et al. SARS-CoV-2 air and surface contamination in residential settings. *Sci. Rep.* **2022**, *12*, 18058. [CrossRef]
13. Martinot, M. Standard precautions should include 'safe ventilation' to minimise far-afield airborne transmission in health and social care settings. *Infect. Dis. Health* **2022**, *28*, 135–137. [CrossRef]
14. U.S. Environmental Protection Agency. Ventilation and Respiratory Viruses. 2025. Available online: https://www.epa.gov/indoor-air-quality-iaq/ventilation-and-respiratory-viruses (accessed on 28 October 2025).
15. Duval, D.; Palmer, J.C.; Tudge, I.; Pearce-Smith, N.; O'Connell, E.; Bennett, A.; Clark, R. Long distance airborne transmission of SARS-CoV-2: Rapid systematic review. *BMJ* **2022**, *377*, e068743. [CrossRef] [PubMed]
16. Ministry of Land, Infrastructure, Transport and Tourism (Japan). Summary of the White Paper on Land, Infrastructure, Transport and Tourism in Japan, 2022. 2022. Available online: https://www.mlit.go.jp/en/statistics/content/001579732.pdf (accessed on 28 October 2025).
17. Kawamura, M.; Ozaki, A.; Arima, Y.; Kuma, Y.; Abe, G.; Isoya, R. Indoor thermal environment and the effectiveness of central air-conditioning in a typical Japanese house under future climate. In Proceedings of the ASim Conference 2024: 5th Asia Conference of IBPSA, Osaka, Japan, 8–10 December 2024; pp. 427–434. [CrossRef]
18. Kishi, T.; Lee, S.; Asano, Y. Adjusting air flow rate for blower fan on central air-conditioning system for residential building: Effect of variable air volume control on thermal environment in a detached house during winter. *J. Environ. Eng. Trans. AIJ* **2020**, *85*, 37–44. [CrossRef]
19. Lee, S.; Kishi, T.; Asano, Y. Applicability of the whole-house air-conditioning system in cold climate district. *E3S Web Conf.* **2019**, *111*, 06036. [CrossRef]
20. ASHRAE. Position Document on Infectious Aerosols. Available online: https://www.ashrae.org/about/position-documents (accessed on 28 October 2025).
21. Etheridge, D.W.; Sandberg, M. *Building Ventilation: Theory and Measurement*; Wiley: Hoboken, NJ, USA, 1996.
22. Dols, W.S.; Polidoro, B.J. *CONTAM User Guide and Program Documentation Version 3.4*; NIST Technical Note 1887r1; National Institute of Standards and Technology: Gaithersburg, MD, USA, 2020. [CrossRef]
23. Feustel, H.E. COMIS—An international multizone air-flow and contaminant transport model. *Energy Build.* **1999**, *30*, 3–18. [CrossRef]
24. Nazaroff, W.W. Indoor particle dynamics. *Indoor Air* **2004**, *14*, 175–183. [CrossRef]
25. Lai, A.C.K.; Nazaroff, W.W. Modeling Indoor Particle Deposition from Turbulent Flow onto Smooth Surfaces. *J. Aerosol Sci.* **2000**, *31*, 463–476. [CrossRef]
26. Hinds, W.C.; Zhu, Y. *Aerosol Technology: Properties, Behavior, and Measurement of Airborne Particles*, 2nd ed.; Wiley: Hoboken, NJ, USA, 1999.
27. Azimi, P.; Stephens, B. HVAC filtration for controlling infectious airborne disease transmission in indoor environments: Predicting risk reductions and operational costs. *Build. Environ.* **2013**, *70*, 150–160. [CrossRef]
28. Thatcher, T.L.; Lai, C.K.A.; Moreno-Jackson, R.; Sextro, R.G.; Nazaroff, W. Effects of room furnishings and air speed on particle deposition rates indoors. *Atmos. Environ.* **2002**, *36*, 1811–1819. [CrossRef]
29. Miller, S.L.; Leiserson, K.; Nazaroff, W.W. Nonlinear Least-Squares Minimization Applied to Tracer Gas Decay for Determining Airflow Rates in a Two-Zone Building. *Indoor Air* **1997**, *7*, 64–75. [CrossRef]
30. Okuyama, H.; Onishi, Y.; Tanabe, S.-I.; Kashihara, S. Statistical data analysis method for multi-zonal airflow measurement using multiple kinds of perfluorocarbon tracer gas. *Build. Environ.* **2009**, *44*, 546–557. [CrossRef]
31. Townsend, A.; Rudd, A.; Lstiburek, J. A calibrated multi-zone airflow model for extension of ventilation system tracer gas testing. *ASHRAE Trans.* **2009**, *115*, 924–942.
32. Howard-Reeds, C.; Wallace, L.A.; Emmerich, S.J. Effect of ventilation systems and air filters on decay rates of particles produced by indoor sources in an occupied townhouse. *Atmos. Environ.* **2003**, *37*, 5295–5306. [CrossRef]
33. He, C.; Morawska, L.; Gilbert, D. Particle deposition rates in residential houses. *Atmos. Environ.* **2005**, *39*, 3891–3899. [CrossRef]
34. GitHub. Iguchi Lab Vtsim: Text.md. Available online: https://github.com/iguchi-lab/vtsim/blob/main/text.md (accessed on 28 October 2025).
35. Peng, Z.; Jimenez, J.L. Exhaled CO_2 as a COVID-19 Infection Risk Proxy for Different Indoor Environments and Activities. *Environ. Sci. Technol. Lett.* **2021**, *8*, 392–397. [CrossRef]
36. Riley, E.C.; Murphy, G.; Riley, R.L. Airborne spread of measles in a suburban elementary school. *Am. J. Epidemiol.* **1978**, *107*, 421–432. [CrossRef]
37. Li, Y.; Qian, H.; Hang, J.; Chen, X.; Cheng, P.; Ling, H.; Wang, S.; Liang, P.; Li, J.; Xiao, S.; et al. Probable airborne transmission of SARS-CoV-2 in a poorly ventilated restaurant. *Build. Environ.* **2021**, *196*, 107788. [CrossRef] [PubMed]

38. Noakes, C.J.; Sleigh, P.A. Mathematical models for assessing the role of airflow on the risk of airborne infection in hospital wards. *J. R. Soc. Interface* **2009**, *6*, S791–S800. [CrossRef]
39. Buonanno, G.; Stabile, L.; Morawska, L. Estimation of airborne viral emission: Quanta emission rate of SARS-CoV-2 for infection risk assessment. *Environ. Int.* **2020**, *141*, 105794. [CrossRef]
40. Lai, A.C.K. Particle deposition indoors: A review. *Indoor Air* **2002**, *12*, 211–214. [CrossRef]
41. Okuyama, K.; Kousaka, Y.; Yoshida, T. Behavior of aerosols undergoing brownian coagulation, brownian diffusion and gravitational settling in a closed chamber. *J. Chem. Eng. Jpn.* **1976**, *9*, 140–146. [CrossRef]
42. Kim, J.; Mulholland, G.; Kukuck, S.; Pui, D. Slip correction measurements of certified PSL nanoparticles using a nanometer differential mobility analyzer (nano-DMA) for Knudsen number from 0.5 to 83. *J. Res. Natl. Inst. Stand. Technol.* **2005**, *110*, 31–54. [CrossRef] [PubMed]
43. Sherman, M.H. Tracer-gas techniques for measuring ventilation in a single zone. *Build. Environ.* **1990**, *25*, 365–374. [CrossRef]
44. Watty Co., Ltd. HYPM Wireless PM Sensor—Specifications. 2019. Available online: https://watty.co.jp/wp-content/uploads/2019/06/HYPM.pdf (accessed on 25 December 2025).
45. Otsuka Pharmaceutical Factory, Inc. Oral Rehydration Solution OS-1 Series—Nutrition Facts (per 100 mL). Available online: https://www.os-1.jp/en/ (accessed on 25 December 2025).
46. Yanagi, U.; Fukushima, N.; Nagai, H.; Ye, H.; Kano, M. Bioaerosol Sensor for In Situ Measurement: Real-Time Measurement of Bioaerosol Particles in a Real Environment and Demonstration of the Effectiveness of Air Purifiers to Reduce Bioaerosol Particle Concentrations at Hot Spots. *Atmosphere* **2023**, *14*, 1656. [CrossRef]
47. Beimdiek, J.; Schmid, H.-J. Evaluation of Surrogate Aerosol Experiments to Predict Spreading and Removal of Virus-Laden Aerosols. *Atmosphere* **2024**, *15*, 305. [CrossRef]
48. Zaatari, M.; Novoselac, A.; Siegel, J. The relationship between filter pressure drop, indoor air quality, and energy consumption in rooftop HVAC units. *Build. Environ.* **2014**, *73*, 151–161. [CrossRef]
49. Rudnick, S.N.; Milton, D.K. Risk of indoor airborne infection transmission estimated from carbon dioxide concentration. *Indoor Air* **2003**, *13*, 237–245. [CrossRef] [PubMed]
50. Saad, M.A.; Hassan, A.; Hanafy, A.; Salem, M.; William, M. Assessing HVAC airflow modulation strategies to reduce short-term aerosol transmission in office environments. *Sci. Rep.* **2025**, *15*, 23911. [CrossRef]
51. Chahardoli, S.; Tak, M.S.N.; Lesan, M.; Mousavi, E.; Bhattacharya, A. Analysis of the Effects of a Swing Door Opening on Indoor Airflow Fields—An Experimental Study. *Buildings* **2025**, *16*, 54. [CrossRef]
52. *NISTIR 5559*; Indoor Air Quality Impacts of Residential HVAC Systems: Phase II. A Report: Baseline and Preliminary Simulations. National Institute of Standards and Technology: Washington, DC, USA, 1995. Available online: https://nvlpubs.nist.gov/nistpubs/Legacy/IR/nistir5559.pdf (accessed on 28 October 2025).
53. Siegel, J. Primary and secondary consequences of indoor air cleaners. *Indoor Air* **2016**, *26*, 88–96. [CrossRef] [PubMed]
54. Pantelic, J.; Tham, K.W. Adequacy of air change rate as the sole indicator of an air distribution system's effectiveness to mitigate airborne infectious disease transmission caused by a cough release in the room with overhead mixing ventilation: A case study. *HVAC&R Res.* **2013**, *19*, 947–961. [CrossRef]
55. Du, L.; Batterman, S.; Godwin, C.; Chin, J.-Y.; Parker, E.; Breen, M.; Brakefield, W.; Robins, T.; Lewis, T. Air Change Rates and Interzonal Flows in Residences, and the Need for Multi-Zone Models for Exposure and Health Analyses. *Int. J. Environ. Res. Public Health* **2012**, *9*, 4639–4661. [CrossRef]
56. Thornburg, J.W.; Rodes, C.E.; Lawless, P.A.; Stevens, C.D.; Williams, R.W. A pilot study of the influence of residential HAC duty cycle on indoor air quality. *Atmos. Environ.* **2004**, *38*, 1567–1577. [CrossRef]
57. Walker, I.S.; Dickerhoff, D.J.; Faulkner, D.; Turner, W.J.N. System Effects of High Efficiency Filters in Homes. Lawrence Berkeley National Laboratory; 2013. LBNL-6144E. Available online: https://eta-publications.lbl.gov/sites/default/files/lbnl-6144e.pdf (accessed on 25 December 2025).
58. Nassif, N. The impact of air filter pressure drop on the performance of typical air-conditioning systems. *Build. Simul.* **2012**, *5*, 345–350. [CrossRef]
59. Stephens, B.; Novoselac, A.; Siegel, J.A. The Effects of Filtration on Pressure Drop and Energy Consumption in Residential HVAC Systems (RP-1299). *HVAC&R Res.* **2010**, *16*, 273–294. [CrossRef]
60. Ward, M.; Siegel, J.A. Modeling filter bypass: Impact on filter efficiency. In Proceedings of the ASHRAE Winter Conference, Orlando, FL, USA, 5–9 February 2005.

Disclaimer/Publisher's Note: The statements, opinions and data contained in all publications are solely those of the individual author(s) and contributor(s) and not of MDPI and/or the editor(s). MDPI and/or the editor(s) disclaim responsibility for any injury to people or property resulting from any ideas, methods, instructions or products referred to in the content.